PROCEEDINGS, Thirty-Seventh Workshop on Geothermal Reservoir Engineering
Stanford University, Stanford, California, January 30 - February 1, 2012
SGP-TR-194

WHY GEOTHERMAL ENERGY RESEARCH NEEDS STATISTICAL SEISMOLOGY

C. E. Bachmann, S. Wiemer, B.P. Goertz-Allmann, B. Mena and F. Catalli

ETH Zurich
Swiss Seismological Service
Sonnegstrasse 5, 8092 Zurich, Switzerland
e-mail: bachmann@sed.ethz.ch

ABSTRACT

Hydraulic fracturing is an increasingly utilized technology to enhance the extraction of hot water or gas from a subsurface reservoir. Fluids are pressed into the reservoir formation from a treatment well at high pressures to open fractures and hence increase the permeability of the reservoir. Monitoring the seismic emission associated with the fluid injection allows to estimate the stimulated reservoir volume, and hence the effectiveness of the treatment. However, oftentimes little is known about the mechanical properties of the reservoir rocks, making it difficult to predict the response of the medium to the fluid injection. On the one hand, one would like to ensure that the fluid injection operation alters the medium sufficiently to make the reservoir economic, and on the other hand it needs to be insured that the magnitude of induced seismic events does not exceed values where shaking can affect surface infrastructure. A proper estimation of the in-situ mechanical properties of the reservoir is therefore necessary for an assessment of both the economics of reservoir treatment as well as the associated seismic hazard at the surface. We introduce ISHA – a probabilistic hazard assessment for induced seismicity, which combines statistical and physics-based models to determine the seismic hazard during the different stages of an EGS experiment. Statistical models have the advantage that they can easily be adapted to the particular conditions of the induced seismicity and that many have been previously tested for other seismic sequences. These models can then be enriched by first order physical models, for example of the pore pressure distribution or the total flow rate. We show examples from an EGS project in Basel, Switzerland, where 3,500 events were located within a volume of approximately 2 km³ at a depth of 4-5 km. We then investigate the spatio-temporal variability of the earthquake size distribution, characterized by the b-value, and find significant variations ranging from high values close to the injection point to lower values further away. Additionally, the b-value changes from high values during the fluid injection to lower values later on. A model, simulating the pore pressure diffusion and relating the event-sizes to the differential stress via an inverse relationship established for tectonic events, aims to evaluate this observation of the b-value distribution. The model implies that high pore pressures lead to high b- values as preferably events with smaller sizes are induced. Moderate pressures lead to values of b similar to the regional average. Since pore pressures decline as a function of distance to the injection point, the probability of observing a large magnitude event thus increases with distance. We are therefore able to establish a link between the seismological observables and the geomechanical properties of the source region and thus a reservoir. Understanding the geomechanical properties is essential for estimating the probability of exceeding a certain magnitude value in the induced seismicity and hence the associated seismic hazard of the operation.

INTRODUCTION

Enhanced Geothermal Systems (EGS) represent a promising alternative for clean energy. For such systems, two boreholes are drilled to depths of below 3 km into the basement, between which a fluid, typically water, is circulated to extract the heat at temperatures well above 100°C. The fluid is pumped at high pressure into the first borehole, to increase the permeability of the rock; a process called reservoir stimulation. This process is accompanied by thousands of micro-earthquakes, their hypocenters reveal critical information about the ongoing evolution of the reservoir. Few events eventually happen to be large enough to be felt at the surface, creating nuisance for the population or even damage to the building stock. The seismic hazard and risk associated with the induced seismicity is in some cases estimated as too high to be acceptable for society. Induced seismicity is currently the largest obstacle to the widespread installation of EGS systems near urban centers (Giardini, 2009).

The EGS project in Basel (Switzerland) in 2006 was terminated after a magnitude ML 3.4 event occurred which was widely felt by the public. A seismic risk study (Baisch et al, 2009) was conducted a posteriori and concluded that the risk was too high to be

acceptable so the project had to be abandoned. To prevent such a scenario, an alarm-system was in place in Basel, a so-called traffic-light-system. This defined actions of this system are based on public response, observed local magnitude and peak ground velocity. According to this system, the fluid injection was reduced and then terminated a few hours before the ML 3.4 event. However, the system could not prevent the large event and the following determination of the project.

Here we introduce a new approach, where we asses the hazard in (pseudo) real-time and update it during the fluid injection. To model the seismicity, we use statistical models and more physics-based models. We apply different updating strategies and compare the performance of the model to find either the best-suiting one or to create a hybrid model.

We investigate the spatio-temporal variability of the earthquake size distribution, characterized by the b-value, to analyze the potential for large magnitude events. We introduce a geomechanical model that recreates the size distribution and can be used to determine the probability for large magnitude events.

DATA

Here we analyze data from a commercial geothermal project in Basel, Switzerland from 2006. This project was conducted by Geothermal Explorers Limited (GEL). Figure 1 indicates the location of the borehole within the city of Basel and the location of the seismic network.

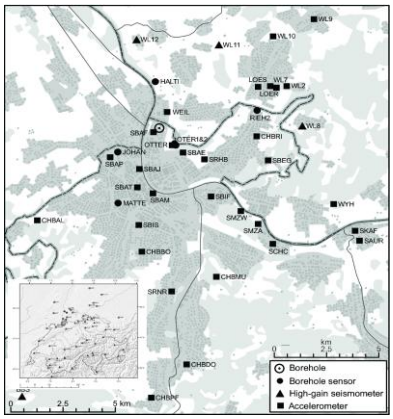

Figure 1: Overview of the study region with all seismic stations. Different symbols show borehole and strong motion stations maintained by either Geothermal Explorers or the Swiss Seismological Service. The inset indicates the location of all seismic stations in Switzerland with the high density of stations around Basel

Fluid was injected during six days from 2. December 2006 to 8. December. The seismicity was recorded by a six-sensore borehole network and a adapted "traffic light system" was used to monitor the ongoing seismicity (Häring et al, 2008). Predefined levels determined actions according to the (1) public response, (2) the observed local magnitude and (3) peak ground velocity (PGV). According to this system, the injection rate was first reduced and then terminated after two events with magnitudes greater than M_L 2.5 were registered. An earthquake with magnitude M_L 3.4, recorded a few hours after the shut-in, lead to the bleed-off of the borehole.

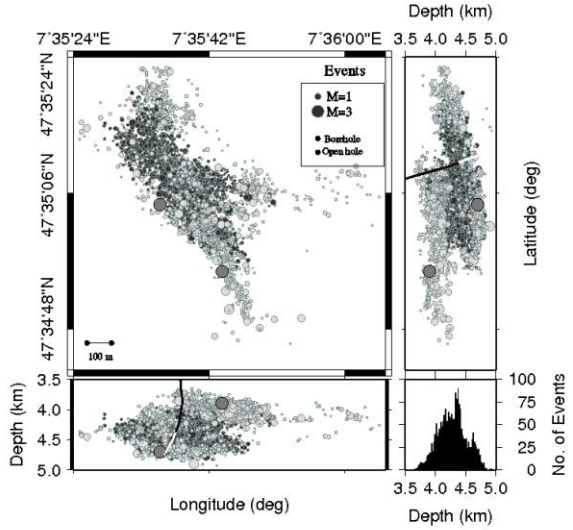

Figure 2: Distribution of the events in plane view (top left panel) and as depth distributions (EW lower panel and NS right panel). Circle sizes are scaled by magnitude; events with magnitudes above 3 are highlighted with darker colors. Events in black occurred during the injection and events in gray after water injection was terminated. The borehole is indicated; the darker part is cased and the lighter part is open.

In total about 11'000 events were recorded, of which around 3'500 were located (Figure 2). For our analysis we use the moment magnitudes provided by GEL. These range from M_W 0.1 to 3.2, with three events above M_W 3 (occurring 0.22, 38 and 55 days after the termination of the injection).

METHOD

Induced Seismicity Hazard Assessment

Traditional Probabilistic Seismic Hazard Assessments (PSHA) quantifies the potential ground shaking due to earthquakes. These approaches determine the probability of exceeding a certain ground velocity for a long period of time (e.g.

Giardini et al., 2004, Wiemer et al., 2009). They are based on historic earthquake catalogs, zonation models and recurrence time models. While this hazard is determined for the longterm and is stable over this period, the hazard associated with induced seismicity is relatively short-term and changes strongly over time.

First estimations of time-varying hazard assessments have been done for aftershock sequences (Gerstenberger et al., 2005, Wiemer & Wyss, 2000).

Here we expand this approach and introduce Induced Seismicity Hazard Assessment (ISHA) to determine the hazard specifically related to induced seismicity. The seismic hazard varies with time during an EGS project. We can distinguish between four different periods for which the hazard needs to be assessed: I) The planning period, II) the reservoir stimulation, III) the operation period and IV) the post-operation period. The hazard during the first period is equal to the hazard in this region determined by traditional PSHA, while for the other three periods the hazard from the injection is added to this background.

Analyzing the seismicity during reservoir stimulation is an important first step towards ISHA. Using methods to determine the validity of the models established in the framework of the Collaboratory Study for Earthquake Predictability (CSEP, http://www.cseptesting.org/), we assess which assumptions lead to the models with the best predictive power.

Forecasting Models

We use three different models to forecast the ongoing seismicity, two are statistical model and one is more physics-based. The statistical models have previously been used to forecast seismic aftershock sequences; we use a model of Reasenberg and Jones (RJ) (Reasenberg & Jones (1989, 1990, 1994)) and an Epidemic Type Aftershock Model (ETAS) (Ogata 1988, Hainzl & Ogata 2005). The more physics-based model was introduced by Shapiro (S) specifically to model induced seismicity. While two of these models (ETAS and S) incorporate the applied flow rate, one does not (RJ).

The RJ model is based on the Omori law and the Gutenberg-Richter law and combines them both to determine the rate λ for events with magnitudes above M_c at time t:

$$\lambda(t, M_c) = \frac{10^{a+b(M_m - M_c)}}{(t+c)^p} \qquad (1)$$

The Reasenberg and Jones model is the basis of the Short-Term Earthquake Probability (STEP) model (Woessner et al., 2010).

We use an ETAS model of Ogata (1988). The rate of aftershocks induced by an event occurring at time t with magnitude M_i is given by:

$$\lambda_t(t) = \frac{K}{(c+t-t_i)^p} 10^{\alpha(M_i - M_{min})} \qquad (2)$$

for time t > ti . The parameters *c* and *p* are empirical parameters and *K* and α describe the productivity of the sequence. The total occurrence rate is the sum of the rate of all preceding earthquakes and a constant background rate. We consider that the forcing term should depend on the applied injection flow rate Fr. According to Shapiro & Dinske (2009), we can model the fluid-triggered event rate as proportional to the injection rate. We therefore modify the background to be:

$$\lambda_0(t) = \mu + c_f \times F_r(t) \qquad (3)$$

with c_f and μ being free parameters.

Shapiro et al. (2010) introduce a model where the number of events is linked to the the injected fluid volume Q_c:

$$\log N_M(t) = \log Q_c(t) - bM + \Sigma \qquad (4)$$

where *M* is the magnitude, *b* is the b-value of the frequency-magnitude distribution (Gutenberg & Richter, 1942) and Σ is the seismogenic index.

Modeling Approaches

Before we apply and compare the forecast models, we define a common framework in which we apply and test the models. This involves choosing the testing period, the updating strategy and the magnitude range in which to test the forecast. Although these choices are somewhat arbitrary, they can potentially have a significant effect on the outcome of the testing, and they reflect to some extent the requirements of end users. We use the experience of the RELM and CSEP experiments to define the 'rules of the game' and retrospective testing of aftershock sequences (Field 2007; Schorlemmer et al. 2010; Woessner et al. 2011).

For all model classes, we apply two modeling approaches: (1) Use one set of pre-determined parameters from the entire sequence; and (2) Update model parameter values with successively extending the period for assembling data by 6 hr. We choose six hours arbitrary as this is a time period within which actions can be executed.

Performance Evaluation

To quantitatively test the model forecasts in a pseudo-prospective approach, we use the N(umber)-test (Schorlemmer et al. 2007, 2010; Lombardi & Marzocchi 2010; Werner et al. 2010; Woessner et al. 2011). This test compares the total forecast rates with the total number of observed earthquakes in the entire volume and indicates whether the too few or too many events are forecast or if the forecast is consistent with the observation. For example, if the model forecasts 0.5 events and 1 is observed, the cumulative Poisson distribution (PCDF) results in a quantile score of δ= PCDF (1, 0.5) = 0.910. We reject the forecasts at the 0.05 significance level, thus for δ-values smaller than 0.025 and larger than 0.975. We determine the N-test for each 6-hr bin; the rejection ratio R_N denotes the percentage of test bins that are rejected. In addition, we perform the L(ikelihood)-test (Schorlemmer et al. 2007, 2010). This test evaluates whether the forecast number of events and the distribution in the magnitude bins is consistent with the observation, again assuming the entire volume as one spatial bin. For each magnitude bin we compute the log-likelihoods and sum this to a joint log-likelihood of the forecast. To verify that the joint log-likelihood is consistent with what is expected if the model is correct, we simulate 10'000 synthetic catalogs consistent with the forecast model and compute their log-likelihood values. This distribution of likelihood values is then compared with the observed log-likelihood. The quantile score γ then measures the amount of simulated log-likelihood values that are smaller than the observed log-likelihood. This test is one-sided and we reject a model if γ <0.025 which implies that the observed log-likelihood is much smaller than expected if the model is true. According to the N-Test, we define the rejection ratio R_L that denotes the percentage of test bins that do not pass the L-test.

There are two different approaches on how to find the best-fitting model: (1) We search for the model with the lowest joint log-likelihood (Bachmann et al, 2011) or (2) we weigh all models according to their Akaike weight (Wiemer et al, 2009) and compute a combined model (Mena et al, 2012).

Probability-based alarm-system

Based on the best-fitting model, we can convert the forecast rates into time-dependent probabilities of a given ground motion intensity, using standard procedures introduced originally by Cornell (1968). Hazard is the result of a combination of seismic rates, their frequency-size distribution and the Ground Motion Prediction Equation (GMPE) and its uncertainty. In contrast to the standard hazard assessment, which is computed for recurrence periods of hundreds to thousands of years, we are here interested in short term hazard in the order of hours to days. This is identical to the time-dependent hazard assessment introduced for aftershocks sequences by Wiemer (2000) and used in California (Gerstenberger et al. 2005).

Thresholds for these intensities - and actions according to them - have to be defined beforehand by the authorities and the people in charge.

Spatio-temporal variability of the seismic parameters

An important input to the models mentioned above is the scaling of the earthquake-size distribution, characterized by the so called b-value from the Gutenberg-Richter law.

$$\log N = a - bM \qquad (5)$$

where N is the number of events with magnitudes larger or equal to *M*, *a* describes the productivity of the sequence and *b* the ratio of small to large events.

As the evolution of the induced seismicity is a highly dynamic process, we need to investigate the dataset with respect to both time and space, and to identify the most prominent gradients in the earthquake-size distribution.

To determine the temporal evolution of the b-value, we divide the dataset into the co- and post-injection period and determine and overall b-value for each subset. To calculate the spatial evolution, we introduce a new focus-centered mapping of the b-value. We determine the local completeness M_c using the closest 150 events in space to each event. The completeness is calculated with the maximum curvature method (Woessner and Wiemer , 2005). M_c defines the catalog threshold for determination of the b-value. To determine the b-value with the maximum likelihood method (Bender , 1983; Utsu , 1999), we require at least 25 events with $M \geq M_c$ in each sample.

Geomechanical Model

We develop a geomechanical model to understand the observed systematic behavior of the b-values with space and time. For this, we simulate the induced seismic cloud in space and time under the hypothesis that high b-values are a response to the pore-pressure perturbation.

We distribute potential failure points (called seed faults), representing pre-stressed faults, randomly in a three-dimensional space with the size of one cubic kilometer, centered around the injection point. At each seed point, we assign values for the minimum and maximum principal stress, σ_3 and σ_1, assuming a Gaussian perturbation to a given background stress regime. A stress perturbation like this could be interpreted as due to the variation of elastic parameters (Langenbruch and Shapiro, 2011). We impose a limit on σ_1, so it cannot exceed a maximum

value as defined by the strong crust limit (Zoback, 2007) and on σ_3, such that it cannot be smaller than the hydrostatic pore pressure p_h. Additionally, σ_1 is always larger than σ_3. The stress distribution for one example seed point is shown in Figure 3 a as a Mohr diagram. The distribution of σ_1 and σ_3 is indicated by the gray histograms (actual distribution after application of limiting constraints) and dashed bell curves (nominal perturbation of values).

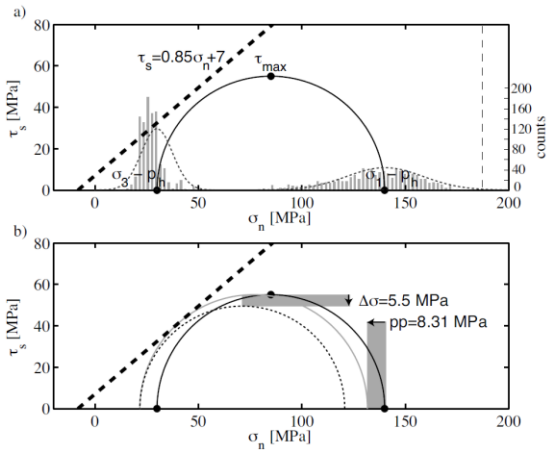

Figure 3: a) Example stress distribution for an average crust at 4.5 km depth at one point in the medium depicted by the Mohr diagram (shear stress τ_s versus normal stress τ_n). The bold dashed line shows the failure envelope. Distribution of stress values around the mean σ_3 and σ_1 are indicated by the dotted line (planned) and the histogram (actual). The vertical dashed line shows the strong crust upper limit for σ_1. b) The black Mohr circle shows the original stress distribution at one point in the medium. The gray circle shows the effective stress of an induced event with the depicted critical pore pressure.

The density of seed faults is a free parameter of the model; it can be adjusted to match the observed amount of seismicity.

We use a time-dependent point pressure source at the injection point. Dinske et al. (2010) introduced an analytical solution to the diffusion equation (Wang, 2000) for the case of a linearly increasing source time function. The pressure-time function is a simplified version of the actual injection pressure pressure in Basel; it is represented as a linearly increasing function over six days. We propagate the pore-pressure through the model space based on linear diffusion in a hydraulically isotropic medium with an effective diffusivity of 0.05 m^2/s. We the solution of Dinske et al., 2011, assuming an effective source radius of 70 m, in order to reach realistic values of the pore-pressure perturbation. The naturally occurring pore-pressure variation in the reservoir due to tides is assumed to be on the order of 2000 Pa (Evans pers. Comm.), we therefore conclude that this is the minimum pressure that is required to trigger an event.

The Mohr circles are shifted towards failure as the normal stresses are reduced due to the pore-pressure evolution. Once the Mohr circle touches the failure envelope, an event is induced. We exploit the observation from laboratory and natural earthquake analysis that b-values are inversely related to the differential stress σ_D (Amitrano, 2003; Schorlemmer et al., 2005), to assign a magnitude to an event. To model the event size of each induced event we link the b-value to σ_D in an inversely proportional relationship ($b = -0.023\ \sigma_D + 4$). We then draw a magnitude randomly from the underlying Gutenberg-Richter relation.

Based on this simple geomechanical simulation, we can also address the question of how large future events will be and how likely they will be. Therefore, we evaluate the synthetic seismicity cloud in time and space for a and b-values within specific time- and distance bins. For each time- or distance bin, we can estimate the probability p of an event exceeding a certain magnitude M as (Wiemer, 2000)

$$p = 1 - e^{1/x} where x = \frac{1}{a - bM} \qquad (6)$$

We choose time bins of 10^5s, moving at 10^4s intervals, and distance bins of 100m, moving across distance in 10m increments.

RESULTS

Forecasting Models

We find that from the three tested models, the Shapiro model leads to the best-fitting individual model. However, a combined model out of all three models using Akaike weights (Wiemer et al, 2009, Kenneth et al, 2002), the performance is even better.

We conclude from this that it is important to include several models in the analysis of induced seismicity and preferably use a combination of them. The temporal evolution of the Akaike weights indicates that the performance of each model changes over time (Figure 5). While the statistical models get higher weights during the injection (first six days), the Shapiro model dominates later on.

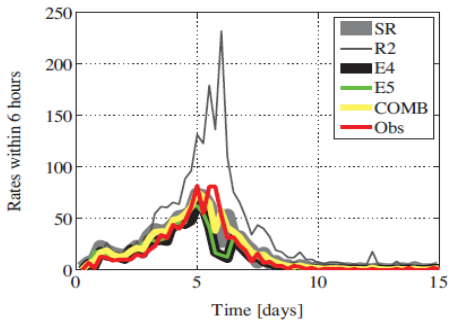

Figure 4: Seismicity rates in time domain. The rates within six hours time bins are based on different approaches of the three models and plotted on top of the observed rates shown in red. The combined model is shown in green.

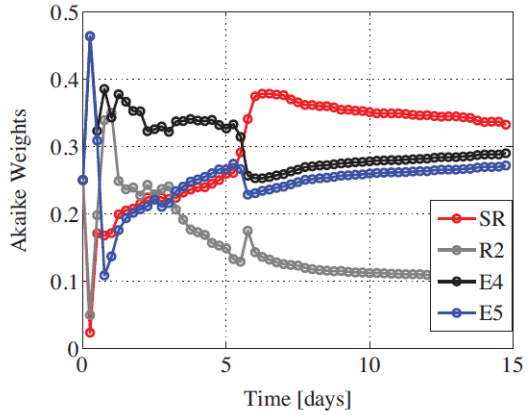

Figure 5: Akaike weights for each forecasting model (SR, R2, E4, E5) computed for six hours time bins.

Spatio-temporal variability of the seismic parameters

We find a substantial decrease of the b-value from 1.58 ± 0.05 to 1.15 ± 0.07 for co- and post-injection events, respectively, using an overall magnitude of completeness of M_c = 0.9. All uncertainties are computed by bootstrapping the data set 100 times and fitting the parameters values to the bootstrap samples.

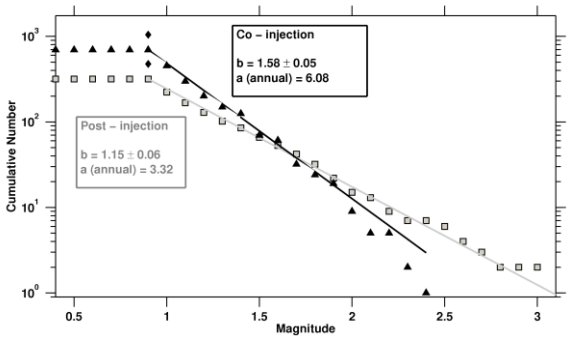

Figure 6: Gutenberg–Richter frequency-magnitude relation for two different sequences. Darker squares show events during the injection, lighter triangles mark events after the termination of water injection. Gutenberg-Richter parameters are indicated for each sequence.

The lower b-value in the post-injection period indicates an increase of the seismic hazard in this period.

The spatial mapping shows a highly varying b-value. The b-value is highest close to the injection point and lower further out. Dividing the map into the co- and post-injection period indicates again that the overall values are higher during the injection and lower after the termination (Figure 6). Events with magnitudes M $\geq$ 2.5 generally lie within regions of lower b-values (pink stars in Figure 6)

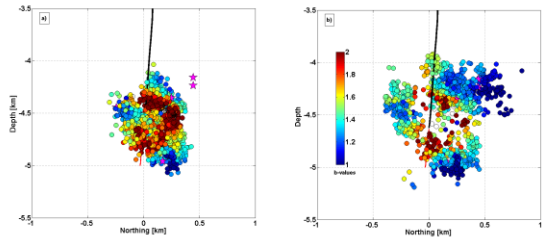

Figure 7: Cross section along the N-S axis, with b-value distribution based on a) co-injection and b) post-injection events. Events with M $\geq$ 2.5 are marked with pink stars.

Geomechanical Model

We find that the simulated seismicity from the geomechanical model shows the similar characteristics as the recorded events from the seismic sequence in Basel. The spatial distribution of the b-value shows highest values close to the injection point and lower values further out. However, the area with the highest b-values is more concentrated around the injection point and we do not find any higher b-value for the post-injection period (b_{max} < 1.6). Figure 8 shows the b-value distribution based on one typical outcome of the simulation, we calculated in total 100 simulations.

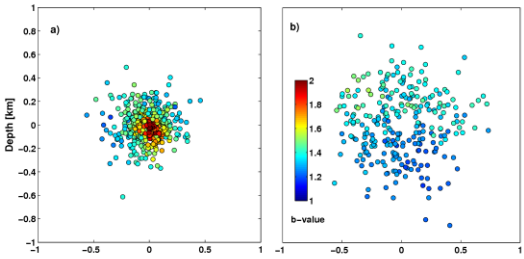

Figure 8: Cross section along the N-S axis, with b-value distribution based on a) co-injection and b) post-injection events for one realization of the geomechanical mode.

Comparing b-value based on all events triggered with pore-pressures above the mean value (2.75 MPa for this simulation) and below shows that the b-value is related the the pore-pressure. We find b_{highP} = 1.45+/-0.01 and b_{lowP} = 1.11+/-0.05.

Figure 9 indicates the probability for an event exceeding M 4 based on 100 simulations of our model. We compare the probability based on our synthetic event cloud with varying b-values (white) with the probability based on an event cloud synthesized from a constant b-value of 1.2 (gray). Error bars indicate the standard deviation obtained from 100 simulations. The probabilistic for large magnitude events increases with time during the injection and decays after the water injection is terminated. With a varying b-value, the mean probability for a M $\geq$ 4 is substantially increased for the time period right after the shut-in (Figure 9a). The maximum probability is also shifted to further out distances from the injection point (Figure 9b).

DISCUSSION AND CONCLUSION

Here we show how the analysis from induced seismicity can profit from statistical seismology. Models introduced to analyze natural seismic sequences are also valid for induced seismicity. While we have to adapt the parameters to fit the different circumstances, the general theories can still be used. By fitting the induced seismic sequence in real-time with statistical and physical models, we can better determine the evolution of seismicity and forecast the rates of seismicity and the expected intensities. Based on predefined thresholds, actions can be executed that are not only based on single observed events alone, but on the integration of the whole observed seismicity.

Analyzing the spatio-temporal evolution of the seismic parameters – such as the b-value – gives us a better insight into the structure of the seismic cloud. While we introduce our simple geomechanical model here mainly to illustrate the link between the b-value and the pore-pressure, it can also be extend in the future into a real time model.

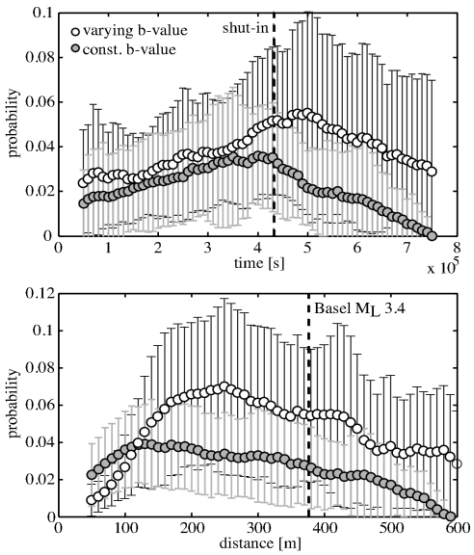

Figure 9: Occurrence probability of M 4 event, varying with a) time and b) radial distance from the injection point for a varying b -value (white) and a constant b -value (gray). The error bar denotes the standard deviation based on 100 simulations of the geomechanical model. The dashed line in a) marks the shut-in time and in b) the location of the largest observed Basel event.

REFERENCES

Amitrano, D., (2003), Brittle-ductile transition and associated seismicity: Experimental and numerical studies and relationship with the b value, *J. Geophy. Res. - Solid Earth*, 108

Bachmann, C.E., S. Wiemer, J. Woessner, and S. Hainzl (2011), Statistical analysis of the induced Based 2006 earthquake sequence: Introducing a probability-based monitoring approach for Enhanced Geothermal Systems, *Geophys. J. Int* ., **186**, 793-807.

Baisch, S., et al. (2009), "Deep heat mining Basel - seismic risk analysis", *Tech. rep., Serianex*.

Cornell, C., (1968). Engineering seismic risk analysis, *Bull. seism. Soc. Am.*, **59(5)**, 1583–1606.

Dinske, C., S. Shapiro and Häring, M. (2010), Interpretation of microseismicity induced by time-dependent injection pressure, *in SEG Expanded Abstracts*, pp. 2125 – 2129

Field, E.H., (2007). Overview of the Working Group for the Development of Regional Earthquake Likelihood Models (RELM), *Seism. Res. Lett.*, **78(1)**, 7–15.

Gerstenberger, M. C., Wiemer, S., Jones, L. M., & Reasenberg, P. A., (2005). Real-time forecasts of tomorrow's earthquakes in California, *Nature* , **435 (7040)**, 328–331.

Giardini, D. (2009), "Geothermal quake risks must be faced", *Nature*, **461**, 848–849.

Giardini, D., Wiemer, S., Fäh, D., and Deichmann, N., (2004), "Seismic hazard assessment of Switzerland, 2004", *Tech. rep., Swiss Seismological Service, ETH Zurich*.

Gutenberg, B. & Richter, C.F., (1942). Earthquake magnitude intensity, energy, and acceleration, *Bull. seism. Soc. Am.*, **32**, 163–191.

Häring, M., U. Schanz, F. Ladner, and B. Dyer (2008), "Characterization of the Basel 1 enhanced geothermal system", *Geothermics*, **37**, 469 – 495.

Hainzl, S. and Ogata, Y., (2005). Detecting fluid signals in seismicity data through statistical earthquake modeling, *J. geophys. Res.*, **110**, B05S07, doi:10.1029/2004JB03247

Kenneth P., K. P. Burnham, and D. R. Anderson (2002), Model selection and multimodel inference: a practical information – theoretic approach, *Springer, New York*

Langenbruch, C., and S. A. Shapiro (2011), Geomechanical interpretation of pore pressures triggering microseismicity, *Expanded Abstracts, 73rd EAGE(P191)*.

Lombardi, A.M. and Marzocchi, W., (2010), The Assumption of Poisson Seismic-Rate Variability in CSEP/RELM Experiments, *Bull. seism. Soc. Am.*, **100(5A)**, 2293–2300.

Mena, B., Wiemer, S and Bachmann, C.E., (2012), Building robust models to forecast the induced seismicity related to geothermal reservoir enhancement, *in preparation*

Ogata, Y., (1999). Seismicity analysis through point-process modeling: a review, *Pure appl. geophys.* , **155** , 471–507.

Ogata, Y., (1988). Statistical-models for earthquake occurrences and residual analysis for point-processes, *J. Am. Stat. Assoc*., **83(401)**, 9–27.

Reasenberg, P.A. And Jones, L.M., (1989). Earthquake hazard after a mainshock in California, *Science*, **243(4895)**, 1173–1176.

Reasenberg, P. and Jones, L., (1990). California aftershock hazard forecasts, *Science*, **247(4940)**, 345–346.

Reasenberg, P. and Jones, L., (1994). Earthquake aftershocks: update, *Science*, **265(5176)**, 1251–1252.

Schorlemmer, D., S. Wiemer, and M. Wyss, (2005), Variations in earthquake-size distribution across different stress regimes, *Nature* , **437** , 539–542.

Schorlemmer, D., Gerstenberger, M.C. ,Wiemer, S., Jackson, D. and Rhoades, D.A., (2007), Earthquake likelihood model testing, S*eism. Res. Lett.*, **87**, 17–29.

Schorlemmer, D., Zechar, J.D.,Werner,M.J., Field, E.H., Jackson, D.D., Jordan, T.H. and Group, T.R.W., (2010), First results of the regional earthquake likelihood models experiment, *Pure appl. Geophys.*, **167(8-9)**, 859–876.

Utsu, T., (1961). A statistical study of the occurence of aftershocks, *Geophys. Mag.* , **3** , 521–605.

Wang, H., (2000), Theory of linear Poroelasticity with Applications to Geomechanics and Hydrogeology, *Princeton Univ. Press*,

Werner, M.J., Zechar, J.D., Marzocchi,W.,Wiemer, S. and CSEP-Italy,Working Grp, (2010), Retrospective evaluation of the five-year and ten-year CSEP-Italy earthquake forecasts, A*nn. Geophys.*, **53(3)**, 11–30.

Wiemer, S. and Wyss, M., (2000), Minimum magnitude of complete reporting in earthquake catalogs: examples from Alaska, the Western United States, and Japan, *Bull. Seismol. Soc.Am.*, **90** , 859–869.

Wiemer, S., Giardini, D., Fäh, D., Deichmann, N., and Sellami, S., (2009), "Probabilistic seismic hazard assessment for Switzerland: best estimates and uncertainties", *J. of Seismology* , **13 (4)**, 449–478.

Woessner, J. & Wiemer, S., (2005), Assessing the quality of earthquake catalogues: estimating the magnitude of completeness and its uncertainty, *Bull. seism. Soc. Am.*, **95(2)**, 684–698.

Woessner, J., Christophersen, A., Zechar, J.D. and Monelli, D., (2010), Building self-consistent, short-term earthquake probability (STEP) models: improved strategies and calibration procedures, *Ann. Geophys.*, **53(3)**, 141–154.

Woessner, J. et al., (2011), A retrospective comparative forecast test on the Landers Sequence, *J. geophys. Res.*, **116**, B05305, doi:10.1029/2010JB007846.

Zoback, M. D. (2007), "Reservoir Geomechanics," *Cambridge University Press, New York*.